

Zinc Binding Drives Sheet Formation by the SAM Domain of Diacylglycerol Kinase δ^{\dagger}

Mary Jane Knight,[‡] Marisa K. Joubert,[§] Megan L. Plotkowski,[‡] Janette Kropat,[‡] Mari Gingery,[‡] Fumio Sakane,^{||} Sabeeha S. Merchant,[‡] and James U. Bowie^{*‡}

[‡]Department of Chemistry and Biochemistry, Institute of Genomics and Proteomics and the Molecular Biology Institute, University of California, Los Angeles, Los Angeles, California 90095-1570, United States, [§]Amgen Inc., Thousand Oaks, California 91320, United States, and ^{||}Department of Chemistry, Graduate School of Science, Chiba University, Chiba, Japan

Received August 6, 2010; Revised Manuscript Received September 20, 2010

ABSTRACT: The diacylglycerol kinase (DGK) family of enzymes plays critical roles in lipid signaling pathways by converting diacylglycerol to phosphatidic acid, thereby downregulating signaling by the former and upregulating signaling by the latter second messenger. Ten DGK family isozymes have been identified to date, which possess different interaction motifs imparting distinct temporal and spatial control of DGK activity to each isozyme. Two DGK family members, δ and η , contain a sterile alpha motif (SAM) domain. The SAM domain of DGK δ 1 forms helical polymers that are important for retaining the enzyme in cytoplasmic puncta, thereby inhibiting activity at the plasma membrane until pathway activation. Because zinc was found to be important for stabilizing the similar SAM polymers of the scaffolding protein Shank-3, we investigated the potential role of zinc in DGK δ SAM domain (DGK δ SAM) assembly. We find that DGK δ SAM binds zinc at multiple sites, driving the organization of the DGK δ SAM into large sheets of polymers. Moreover, a mutant DGK δ containing a SAM domain refractory to zinc binding diminishes the formation of cytoplasmic puncta, shows partially impaired regulation of transport to the plasma membrane, and lacks the ability to inhibit the formation of CopII coated vesicles. These results suggest that zinc may play an important role in the assembly and physiology of the DGK δ isozyme.

Diacylglycerol (DG)¹ serves as an intermediate in lipid metabolism and also acts as a powerful second messenger known to influence cell proliferation and differentiation, at least in part through the allosteric activation of protein kinase C (1). The primary means of downregulating DG in the cell is through DGK-catalyzed formation of phosphatidic acid (PA). PA also serves as a second messenger lipid in signaling pathways that involve metabolic and mitogenic cell responses (2). Both DG and PA levels must, therefore, be tightly regulated. Highly specific spatial and temporal control of DGK activity in different cell types is achieved in part by the presence of diverse regulatory domains attached to the common catalytic core (3). Based on their domain structures, the DGK enzymes can be grouped into five subfamilies (3). DGK enzymes of the type II DGK subfamily (δ , η , κ) are characterized by an N-terminal plekstrin homology (PH) domain and catalytic and accessory domains (4–6). The closely related δ and η members also contain a C-terminal SAM domain (4, 7).

Two splice variants of DGK δ , DGK δ 1 and DGK δ 2, have been identified with divergent cellular distributions and response to stimuli. DGK δ 2 is identical to DGK δ 1 except for the addition of 52 residues at the N terminus. Both DGK δ 1 and δ 2 splice variants can be found in a punctate, cytoplasmic distribution in

the absence of cell stimulation (8, 9). A fraction of the DGK δ 2 puncta colocalize with markers for clathrin-coated vesicles, and DGK δ 2 kinase activity is required for efficient uptake of cell surface receptor cargo into these vesicles (10). The nature of the puncta formed by the δ 1 isoform is unknown, but DGK δ 1 has also been shown to associate with the endoplasmic reticulum membrane and inhibit anterograde ER-to-Golgi transport when overexpressed (11). DGK δ 1 relocates to the plasma membrane upon stimulation with 12-*O*-tetradecanoylphorbol 13-acetate (TPA) (8). DGK δ 1 deficiency has also been implicated in the development of hyperglycemia-induced insulin resistance and thus may contribute to the progression of type II diabetes (12).

The DGK δ SAM domain, which is found in both splice variants, is required for association of DGK δ 1 with the ER (11), inhibition of CopII-coated vesicle formation (10), and retention of DGK δ 1 in its punctate, cytoplasmic distribution in the absence of stimulation (11). DGK δ SAM forms polymers with features that are quite similar to polymers formed by other SAM domains (13–16). In particular, our earlier crystal structure of DGK δ SAM revealed a left-handed helical polymer with six subunits per turn shown in Figure 1 (17). The subunits within the polymer associate via two distinct surfaces on the SAM domain called the mid-loop (ML) surface and the end-helix (EH) surface (13). Mutations in the polymer interface that reduce subunit association affinity lead to a redistribution of DGK δ from the cytoplasmic puncta to the plasma membrane (8), suggesting that polymerization is important for maintenance of the protein in the cytoplasm.

A closely related SAM domain from the rat Shank-3 protein (Shank3SAM) also forms polymers, but these polymers can associate in a side-by-side fashion to create sheets (14). The sheets become highly ordered in the presence of zinc ions.

[†]This work was supported by NIH Grants R01GM093393 and R01CA081000 to J.U.B., and NIH Grant GM42143 to S.S.M.

*Address correspondence to this author. Phone: 310-206-4747. Fax: 310-206-4749. E-mail: bowie@mbi.ucla.edu.

Abbreviations: TPA, 12-*O*-tetradecanoylphorbol 13-acetate; DG, diacylglycerol; DGK, diacylglycerol kinase; EM, electron microscopy; EH, end helix; ER, endoplasmic reticulum; ICP-MS, inductively coupled mass spectrometry; MBP, maltose binding protein; ML, mid-loop; PA, phosphatidic acid; PH, plekstrin homology; SAM, sterile alpha motif.

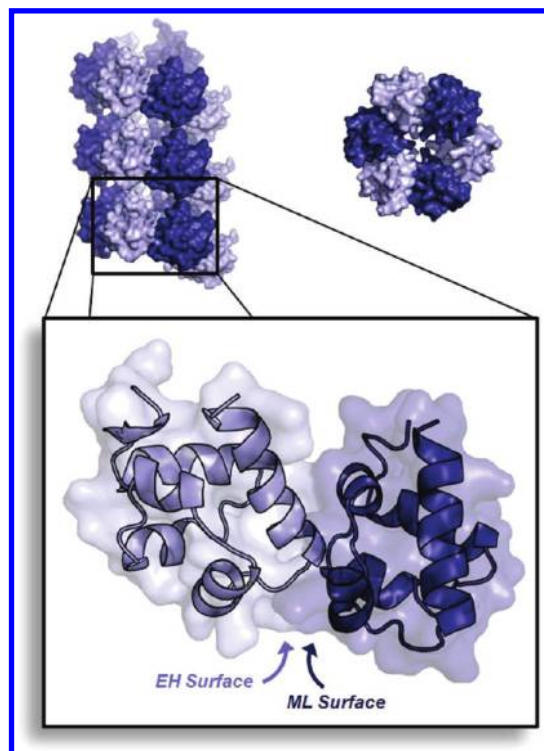


FIGURE 1: The DGK δ SAM polymer. Top left: A space-filling representation of several turns of the helical DGK δ SAM polymer perpendicular to the polymer axis. Every other subunit is colored light blue or dark blue. Top right: The polymer viewed down the polymer axis. Bottom: Two subunits of the polymer shown in isolation. The EH SAM interaction surface resides on the light blue subunit, and the ML surface resides on the dark blue subunit.

We therefore hypothesized that zinc might also serve to organize DGK into a higher order assembly and might have an impact on enzyme localization and function. Here we show that DGK δ -SAM does indeed bind zinc, leading to sheet formation that may be important for its biological function.

EXPERIMENTAL PROCEDURES

Cloning. DGK δ 1-WT (residues 1097–1163 of the full-length protein which corresponds to residues 1–66 of the SAM domain) was inserted into the pMALc2x vector (Novagen) using *Sa*I and *Hind*III sites to generate MBP-DGK δ SAM-WT. Mutations and deletions were introduced into all constructs using QuickChange mutagenesis (Stratagene) and confirmed by sequencing (Genewiz).

For the DGK δ SAM-V52E and DGK δ SAM-E35G constructs that were used in tag-free applications, the DGK δ SAM domain (containing the residues specified above) was PCR amplified and ligated into a modified pET3c vector that contains the expression leader sequence MEKTR followed by a His₆ tag and a tobacco etch virus (TEV) protease site, ENLYFQG, N-terminal to the DGK δ SAM sequence such that the His₆ tag could be removed. The E35G and V52E mutations were introduced as described above. After cleavage the DGK δ SAM-V52E protein contains an added N-terminal G and C-terminal RD.

pEGFP-DGK δ -WT (GFP-DGK δ 1-WT) and pEGFP-DGK δ 1(V52E) (GFP-DGK δ 1-V52E) constructs were described previously (17). The GFP-DGK δ 1- Δ SAM was generated by deleting residues 1097–1163 via QuickChange mutagenesis using primers with complementary sequences to the immediately upstream and downstream portions of the DGK δ construct.

Protein Purification. All MBP-fusion constructs were expressed in ARI814 cells. The cells were grown at 37 °C in LB media supplemented with 100 μ g/mL ampicillin until the cell density reached an OD₆₀₀ of 0.8. Protein expression was induced with 1 mM isopropyl β -D-galactopyranoside (IPTG) and incubated at 37 °C for an additional 2 h at which point the cells were harvested by centrifugation. Cell pellet (40 g) was resuspended in 140 mL of 20 mM Tris (pH 7.5), 200 mM NaCl, 1 mM TCEP, and 5 mM MgCl₂ containing lysozyme (1 mg/mL), Dnase I (10 μ g/mL), 0.5 mM PMSF, and eight tablets of Complete protease inhibitor (Roche). The cells were lysed by sonication, and the lysate was centrifuged at 27000g for 45 min. The supernatant was incubated with 50 mL of amylose resin (New England Biolabs) for 1 h at 4 °C. The resin was poured into a column and washed with 7 column volumes of 20 mM Tris (pH 7.5), 300 mM NaCl, and 1 mM TCEP, and protein was eluted in 20 mM Tris (pH 7.5), 200 mM NaCl, and 1 mM TCEP, with 10 mM maltose. In order to separate proteolyzed, free MBP from the intact fusion protein, the eluted protein was then applied to a 5 mL IMAC-HP column (GE Biosciences) charged with zinc acetate, and the bound protein was eluted in 15 mL of 20 mM Tris (pH 7.5), 200 mM NaCl, and 1 mM TCEP, with 500 mM imidazole. MBP-DGK δ SAM^{ZnMut} did not bind the zinc column but displayed essentially no proteolysis so this further purification step was not necessary. The protein was dialyzed at 4 °C for 4 h against 2 L of 20 mM Tris (pH 7.5), 200 mM NaCl, and 1 mM TCEP and transferred to 2 L of the same buffer for overnight dialysis. Dialyzed protein was concentrated using an Amicon Ultra centrifugal filter concentrator unit (Millipore).

The DGK δ SAM-V52E construct was transformed into BL21-(DE3) cells and grown at 37 °C in LB media supplemented with 100 μ g/mL ampicillin until the cell density reached an OD₆₀₀ of 0.6. Cells were induced with 1 mM IPTG and incubated at 37 °C for an additional 5 h at which point they were harvested by centrifugation. Cell pellet (40 g) was resuspended in 140 mL of 20 mM Tris (pH 7.5), 300 mM NaCl, 5 mM MgCl₂, and 1 mM TCEP, containing 0.5 mM PMSF, lysozyme (1 mg/mL), and Dnase I (10 μ g/mL). Cells were lysed as described above. Cell supernatant was applied to 3 mL of Ni-NTA Superflow resin (Qiagen) and incubated for 1 h. Resin was washed with 200 mL of the same buffer and eluted with buffer containing 300 mM imidazole. The His₆ tag was cleaved with TEV protease S219V at 0.5 mg/mL DGK-SAM TEV at a mole ratio of 5:1 TEV to DGK δ SAM, and the reaction was incubated with mixing for 24 h at 4 °C. The cleaved mixture underwent two rounds of subtractive Ni-NTA affinity chromatography to remove the His tag, protease, and uncleaved substrate. Cleaved protein was dialyzed and concentrated as described above.

Turbidity Assay. Tag-free DGK δ SAM-E35G protein (200 μ L of 38 μ M) in 20 mM Tris (pH 7.5) and 50 mM NaCl was incubated with either 38 μ M zinc acetate or 1 mM EDTA or a sequential combination of the two with a 20 min incubation between additions. After 24 h at 4 °C, samples were transferred to a UV/vis transparent 96-well microtiter plate, and A₃₅₀ was measured using a SpectraMax Plus microplate reader (Molecular Devices). Samples were prepared in triplicate, and the average was calculated. In order to construct a turbidity curve for increasing concentrations of zinc acetate, 150 μ L samples of 20 μ M tag-free DGK δ SAM-E35G were individually incubated with 5 μ L of a dilution series of zinc acetate such that the range of final zinc concentrations spanned from 0 to 57 μ M. After 24 h incubation at 4 °C, samples were assayed as above.

Gel Filtration. MBP-DGK δ SAM-WT (500 μ L of 16.5 μ M), MBP-DGK δ SAM^{ZnMut}, and MBP protein in 20 mM Tris (pH 7.5) and 500 mM NaCl were incubated with 1 mM EDTA for 30 min at room temperature. Protein solutions were then centrifuged for 10 min at 16000g. Protein was loaded onto a Superdex 200-10/300GL gel filtration column (Amersham Biosciences) at 0.5 mL/min.

Zinquin Fluorescence Assay. Samples (200 μ L) of 37 μ M tag-free DGK δ SAM-WT protein in 20 mM Tris pH 7.5, 50 mM NaCl were independently incubated with either 7.4 μ M zinc acetate or zinc-free buffer for 30 min at room temperature, and samples were centrifuged to separate the precipitated fraction. Samples were prepared in triplicate. Supernatant was transferred to a separate tube, and precipitate was washed with three successive 500 μ L washes of zinc-free buffer. The precipitated protein was then resolubilized in 200 μ L of 8 M urea. The final urea concentration of all samples (supernatant, precipitated protein fractions, and protein incubated in zinc-free buffer) was adjusted to 6 M urea in 20 mM Tris (pH 7.5) and 50 mM NaCl. Each sample (200 μ L) was then incubated with 50 μ M zinquin ethyl ester and incubated at room temperature for 30 min. Zinquin fluorescence was monitored in 96-well clear-bottom, black-sided plates (Nunc) on a Molecular Devices Spectramax M5 plate reader using an excitation wavelength of 368 nm, an emission wavelength of 510 nm, and a cutoff filter of 495 nm. Protein concentration was measured by absorbance at 280 nm on a Nanodrop spectrophotometer (Thermo Scientific).

Electron Microscopy. Protein samples in 5 mM Tris (pH 7.5), 50 mM NaCl, and 6 M urea were dialyzed into the same buffer without urea either with or without 1 mM zinc acetate. Carbon-coated parlodion support films mounted on copper grids were made hydrophilic immediately before use. Approximately 3 μ L of each protein sample was applied to separate grids and allowed to adhere for several minutes. Grids were rinsed with distilled water and negatively stained with 1% uranyl acetate. Samples were examined in a Hitachi H-7000 electron microscope at an accelerating voltage of 75 kV.

ICP-MS Analysis of Purified MBP-DGK δ SAM Mutants. Five milliliters each of 16 μ M MBP-DGK δ SAM constructs and MBP was dialyzed into 2 L of 20 mM Tris, pH 7.5, 50 mM NaCl, and 1 mM zinc acetate for 24 h and then transferred to 2 L of fresh buffer for an additional 24 h. In the case of the metal competition assay, MBP and MBP-DGK δ SAM-WT were dialyzed into 20 mM Tris, pH 7.5, 50 mM NaCl, 160 μ M zinc sulfate, 160 μ M cobalt sulfate, 160 μ M copper sulfate, 160 μ M manganese sulfate, and 160 μ M magnesium sulfate as above. After metal incubation was complete, samples were dialyzed against 4 L of 20 mM Tris, pH 7.5, and 50 mM NaCl for 10 h followed by three successive transfers into fresh buffer. Samples were transferred to acid-washed 15 mL conical tubes, and ultrapure nitric acid was added to a final concentration of 5%. Samples were incubated at 60 °C until no particulate matter could be observed. Ultrapure water was added to adjust the final nitric acid concentration to 2.4%. Yttrium and gallium were added as internal standards to all samples, and a serial dilution of standard CL-CAL-2 (Claritas) was used to create a standard curve for all metals measured. Samples were analyzed using an Agilent 7500ce Quadrupole ICP-MS. One isotope for each metal (Mg 24, Mn 55, Co 59, Ni 60, Cu 63, and Zn 66) was measured, and total metal occupancy was extrapolated.

Surface Plasmon Resonance. The surface plasmon resonance experiments were performed at 20 °C on a Biacore T100

instrument, essentially as described previously (17). Either MBP-DGKSAM-V52E or MBP-DGKSAM-H38A/V52E was immobilized on a Biacore CM5 sensor chip via EDC/NHS cross-linking, and various concentrations of MBP-DGKSAM-E35G were applied to the chip in 0.01 M HEPES (pH 7.4), 0.15 M NaCl, 3 mM EDTA, and 0.005% surfactant P20 until equilibrium binding was achieved. The resulting binding data were fit to a 1 to 1 binding model using Kaleidagraph software.

Cell Culture and Transfection. Human embryonic kidney (HEK293) cells and Cos7 cells stably expressing Sec13-YFP were maintained at 37 °C in high glucose DMEM (Gibco) supplemented with 10% fetal bovine serum (FBS). To prepare cells for transfection, they were grown on chamber slides (Nunc) for 1 day. Transfections and cotransfections of plasmids (pEGFP-DGK δ 1-WT, pEGFP-DGK δ 1-V52E, pEGFP-DGK δ 1 ^{Δ SAM}, pEGFP-DGK δ 1^{ZnMut}, and mCherry-Clathrin) were carried out using lipofectamine or lipofectamine LTX (Invitrogen) per the manufacturer's instructions. The media were replaced with DMEM supplemented with 10% FBS, and cells were incubated for an additional 2 days before use.

TPA Induction. Cells transfected with either pEGFP-DGK δ 1^{WT} or pEGFP-DGK δ 1^{ZnMut} were washed with PBS, and media were replaced with DMEM containing 10% FBS and 0.1% BSA. After a 3 h incubation, cells were exchanged into the same media containing 0.00, 0.15, 0.30, 0.45, 0.60, 0.75, 0.90, or 1.05 μ M TPA and incubated for 1 h.

Confocal Microscopy. Cells were fixed onto slides for 10 min using 3.7% formaldehyde in PBS, washed twice with PBS, and mounted using ProLong Gold antifade reagent with Dapi (Invitrogen). Cells were visualized using a Leica TCS-SP2 AOBs confocal microscope, and images were processed using Leica confocal software. The estimated ratio of GFP fluorescence in the PM region versus the cytosolic region in the TPA-stimulated cells was determined by taking a line intensity profile through a given cell using the ImageJ software. The PM-region fluorescence was defined as the average fluorescence of the 1 μ m segment that contains a fluorescence signal above background, and the cytosolic-region fluorescence was defined as the average fluorescence of 1 μ m, 0.5 μ m to the interior of the cell from the defined PM region. A PM/cytosol fluorescence ratio was then calculated for each edge of the cell, two ratios per line profile. The averages from three lines drawn at different angles through the cell were then averaged to get an overall average ratio for a given cell. The average ratios from 20 cells of each sample were averaged to obtain overall population averages. A two-tailed *t* test was performed in Microsoft Excel assuming heteroscedastic populations.

RESULTS

DGK δ SAM Binds Zinc. To test whether DGK δ SAM is capable of binding a metal ion with high affinity and specificity, we performed a metal-retention competition assay. We dialyzed a DGK δ SAM-WT-maltose binding protein (MBP) fusion (MBP-DGK δ SAM-WT) into a buffer containing zinc, cobalt, copper, manganese, and magnesium, each in 10-fold molar excess for 46 h. The MBP fusion was utilized as a solubility-enhancing factor. The protein was then dialyzed extensively against metal-free buffer. MBP does not contain a metal binding site and was used as a negative control. Inductively coupled mass spectrometry (ICP-MS) analysis indicates that while MBP retains a negligible amount of any of the metal ions included in the experiment, MBP-DGK δ SAM-WT retains considerable zinc and a small amount of copper (Figure 2A). While the possibility

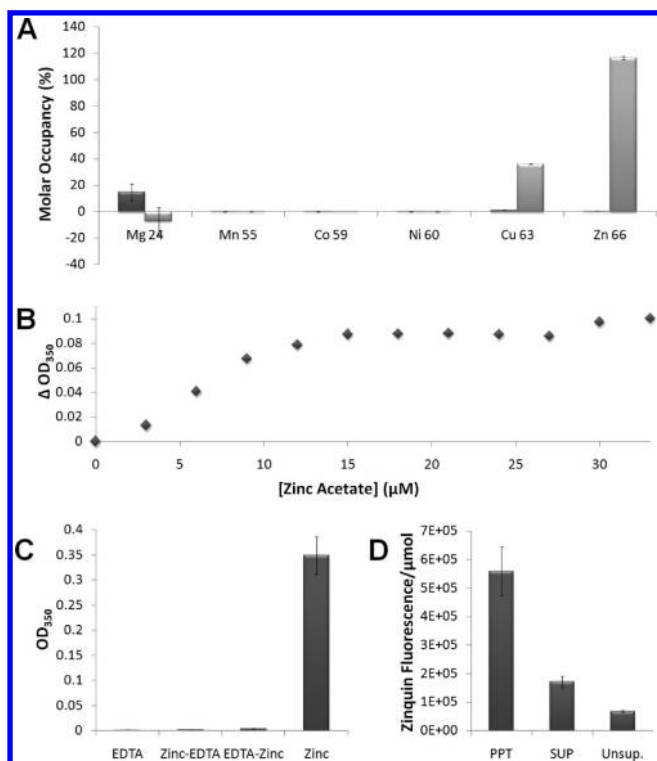


FIGURE 2: Zinc is bound by DGKδSAM and induces a shift to higher molecular weight species. (A) Metal binding by DGKδSAM. DGKδSAM-WT (light gray bars) and MBP (dark gray bars) were incubated with equal concentration of metal sulfate solutions, and the total metal content was determined by ICP-MS. The molar percent occupancy of metal ions in a given protein sample is shown. (B) Zinc binding drives aggregation. The turbidity (A_{350}) of a 20 μ M tag-free DGKδSAM-E35G protein incubated with various concentrations of zinc acetate is shown. (C) Zinc-induced aggregation is reversible. Tag-free DGKδSAM-E35G protein was either incubated with zinc, zinc followed by EDTA, EDTA followed by zinc, or just EDTA. The turbidity after 24 h is shown. (D) Zinc is associated preferentially with insoluble material. 37 μ M tag-free DGKδSAM-E35G protein was incubated in buffer supplemented with 7.4 μ M Zn or without additional Zn supplementation. The zinc-precipitated fraction was separated from the remaining soluble protein, and all samples were denatured and zinc assayed by zinquin fluorescence. The fluorescence per μ mol of protein is shown. “PPT” refers to the zinc-precipitated protein fraction, “SUP” to the remaining soluble supernatant, and “Unsup” to the protein sample incubated in zinc-free buffer.

that there is a copper-specific binding site in addition to one or more separate zinc-binding sites cannot be excluded, the similarity of copper and zinc metalloprotein binding sites (18–22) and the inherently more stable copper–protein ligand interaction per the Irving–Williams series trend (23), combined with the fact that zinc is more abundant than copper in the human body (24), suggests that the retained copper may be the result of promiscuous binding by a zinc-specific site.

A zinc binding site that is self-contained within a single protein subunit can yield a total maximum occupancy of 100%, and a zinc binding site that is shared between two subunits can contribute a total maximum occupancy of 50%. The molar occupancy of zinc observed for the wild-type protein was 116.6% despite extensive dialysis. This suggests that there is at least one high-affinity zinc binding site and potentially additional binding sites, particularly if copper is occupying some fraction of the sites that normally accept zinc.

Zinc Induces Assembly into Sheets. We observed that adding zinc to the MBP-DGKδSAM-WT construct caused a

fraction of the protein to precipitate. This phenomenon allowed us to investigate whether zinc binding could drive the higher order assembly of DGKδSAM, using a simple turbidity assay. DGKδSAM-E35G is a mutant of DGKδSAM that exhibits greatly reduced polymerization as position 35 lies buried in the subunit interface. As shown in Figure 2B,C, when 1 molar equiv of zinc acetate was added to a solution of 38 μ M DGKδSAM-E35G, turbidity increased dramatically, indicating some degree of aggregation. In contrast, maltose binding protein (MBP), which does not bind zinc, showed no increase in turbidity upon zinc addition (not shown). The addition of EDTA to a sample after it reached maximal turbidity caused a reduction in turbidity to nearly the original level, indicating that the aggregation process is reversible. Samples which were incubated with EDTA followed by addition of zinc showed a negligible increase in turbidity. These results suggest that zinc binding may enhance the assembly of DGKδ-SAM. If the aggregates are formed by SAM polymers, zinc binding must be able to overcome the decrease in subunit binding affinity imparted by the E35G mutation.

If we assume that turbidity reflects zinc binding, we can obtain an upper estimate of the zinc dissociation constant (K_d). In particular, 20 μ M DGKδSAM-E35G was incubated with 0–57 μ M zinc acetate solution followed by turbidity measurement. The maximal turbidity response was attained at a zinc concentration of 20 μ M zinc acetate, suggesting stoichiometric zinc binding at this protein concentration (Figure 2B). This indicates that the zinc K_d must be well below 10 μ M.

If zinc causes DGKδSAM precipitation by stabilizing large oligomeric structures, zinc should preferentially associate with the insoluble fraction of the protein. Samples of DGKδSAM-E35G incubated with an excess of zinc are shifted entirely to the insoluble fraction so a limiting concentration of zinc was added to protein samples such that both soluble and insoluble fractions could be isolated. Both fractions were denatured and assayed with zinquin, a zinc-responsive fluorophore, to determine whether the protein populations retained zinc ions. The total normalized fluorescence of the samples per micromole of protein is shown in Figure 2D. The zinc-precipitated fraction does indeed display more than three times as much zinquin fluorescence per micromole of protein than the protein in the soluble fraction. Without zinc supplementation, DGKδSAM-E35G also displays a measurable zinquin signal, suggesting that the purified protein retains some amount of zinc that became bound in the cell or during the course of purification, a further indication of a high-affinity zinc binding site.

To investigate the nature of the zinc-induced aggregate, we examined it by electron microscopy (EM). Figure 3 shows negative stain EM images of DGKδSAM-E35G in the presence and absence of zinc. Gel filtration chromatography indicates that most of the DGKδSAM-E35G protein sample is monomeric in the absence of zinc (not shown), but in the EM field we found occasional polymers that show a propensity to associate side by side forming thin ribbons (Figure 3A). It is possible that these polymer assemblies are assisted by the small amount of zinc retained during purification as described above. In the presence of added zinc, DGKδSAM-E35G organizes into large sheet structures (Figure 3B,C). In the presence of 50 μ M zinc acetate large, folded sheet structures are common, and in 1 mM zinc acetate the grid is entirely covered in large layers of sheets with rare breaks in the continuous structure. A second monomeric mutant of DGKδSAM (DGKδSAM-V52E) was also examined by EM (Supporting Information Figure S1). V52E is a stronger

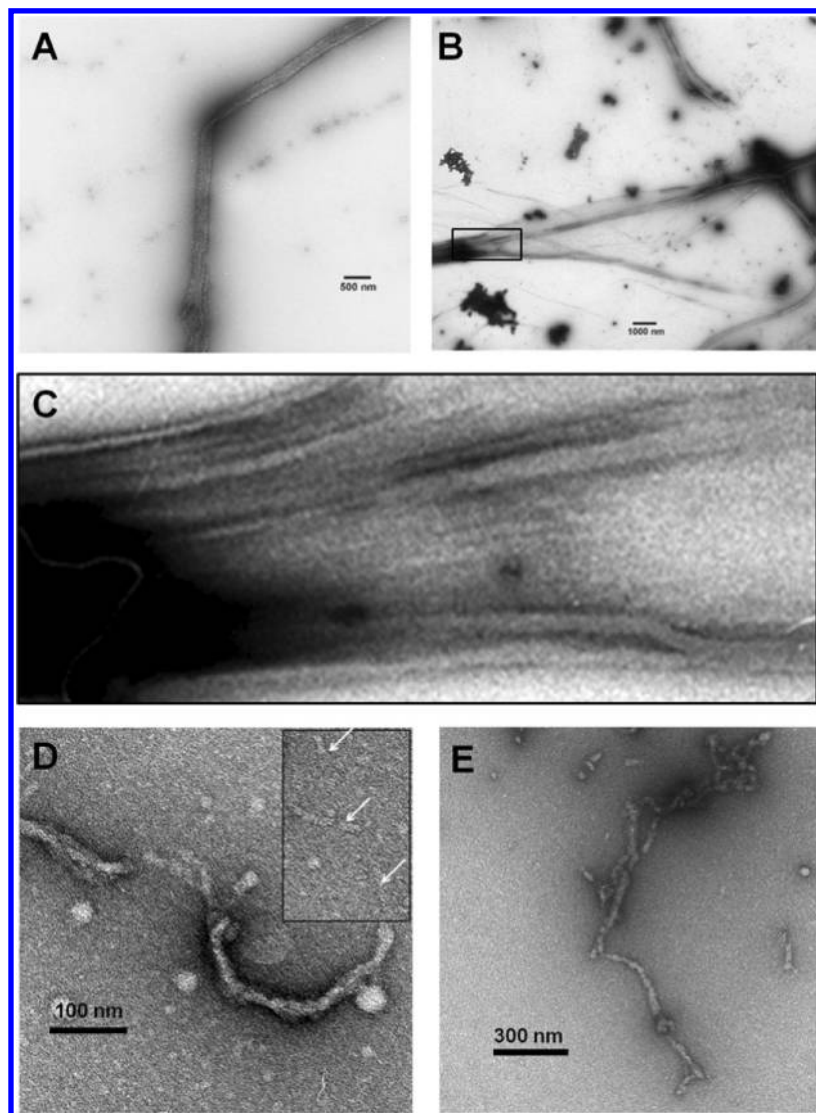


FIGURE 3: Zinc induces formation of DGK δ SAM sheet oligomers. DGK δ SAM protein samples were refolded in the absence or presence of zinc acetate and then visualized by electron microscopy. (A) DGK δ SAM-E35G without added zinc. The protein is almost entirely monomeric, but some polymers are found (perhaps due to residual zinc) with the expected 8 nm diameter, which associate lengthwise to form ribbons. (B) DGK δ SAM-E35G + 50 μ M zinc. Large sheet structures are formed. (C) A close-up view of the boxed portion of frame B. Sheet striations are visible suggesting that the sheets are formed by association of polymers. (D) DGK δ SAM^{ZnMut} without added zinc. A rare, bundled polymer species similar to those seen previously for wild type is shown. Single, unbundled polymers from the same grid shown in the inset are the dominant polymer species (arrows). (E) DGK δ SAM^{ZnMut} + 1000 μ M zinc. Slightly longer, more prevalent polymers are apparent with added zinc, but not large sheets.

monomeric mutation in that a larger percentage of the protein population exists as monomers (17), reflected by the fact that no polymers are visible in zinc-free conditions. After zinc addition, however, large sheet structures visually identical to those seen in the DGK δ SAM-E35G sample appear. While the sheets appear largely smooth and featureless, in both samples the sheet edges are straight, and striations in the sheet structure can be seen in some of the darkly stained regions, supporting a model in which polymers associate longitudinally to form the massive sheets. These sheets thus appear to be quite similar to the sheets observed for Shank3SAM, which are also stabilized by zinc ions.

In the crystal structure of Shank3SAM, helical polymers associated side by side into parallel and antiparallel sheets, which were predicted to approximate the quaternary structure of the sheets visualized by EM (14). As shown in Figure 4, similar packing is also present in the DGK δ SAM-E35G structure (17). If the side-by-side packing elements represent the sheet structure, the DGK δ SAM sheet interface is far more densely packed than

the interface observed for Shank3SAM, due in part to the smaller helical pitch of the DGK δ SAM polymer (Figure 1). This higher packing density is consistent with the low level of detail observed in the micrographs of DGK δ SAM sheet structures as the negative stain would be unable to penetrate deeply into the tightly packed crevasses between subunits and polymers.

Construction of a DGK δ SAM Mutant Refractory to Zinc. The results presented so far indicate that zinc binding can dramatically stabilize higher order oligomerization of DGK δ SAM *in vitro*. In particular, the polymers observed previously can be packed side by side to create sheet structures. To investigate whether zinc-induced sheet formation is important for the biological function of DGK δ , a mutant of DGK δ SAM was constructed that could still form polymers like the wild-type protein but could no longer bind zinc and could therefore not form stable sheets.

To construct a zinc refractory mutant, it was necessary to identify residues involved in zinc binding. Attempts to identify

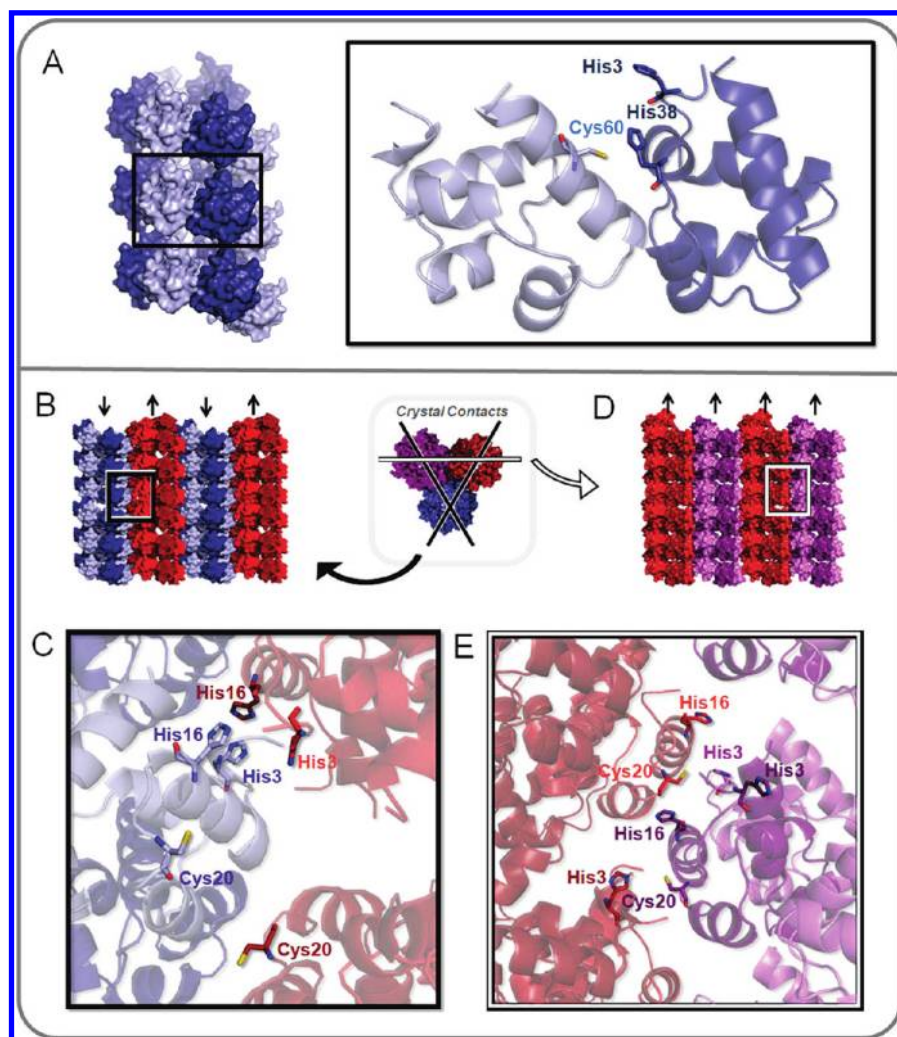


FIGURE 4: Zinc binding residues cluster at both inter- and intrapolymer interfaces. (A) Possible zinc binding residues that cluster in the intrapolymer interface. Left: A space-filling representation of several turns of the helical polymer perpendicular to the polymer axis. Right: Two subunits of the polymer shown in isolation showing Cys60 and His38 side chains. His3 is also displayed because it is on a flexible portion of the protein and could potentially participate in zinc binding. (B–E) Possible zinc binding residues that cluster between polymers. The crystal structure included both parallel and antiparallel association of polymers in its packing, and either one could create sheets. (B) The antiparallel association of helical polymers. (C) Possible zinc binding residues that cluster at the antiparallel interface. (D) The parallel association of polymers. (E) Possible zinc binding residues that cluster at the parallel interface.

the zinc binding residues by obtaining crystals of DGK δ SAM in the presence of zinc were unsuccessful. Moreover, the zinc binding site found in Shank3SAM is not completely conserved in DGK δ SAM, making it unlikely to bind zinc in an identical manner (Supporting Information Figure S2). To circumvent the lack of structural data, Hotpatch (25), a statistical prediction program capable of identifying potential metal binding sites, was employed, providing a list of residues that were most likely to be involved in zinc binding (His3, Cys20, Glu21, His38, Cys60). These residues clustered into two potential Zn sites. One cluster is within the polymer (intrapolymer) and involves residues His38 and Cys60 (Figure 4A). A second cluster involves residues His3 and Cys20 and would be located between polymers (interpolymer), possibly stabilizing the side-by-side assembly of the polymers. As both parallel and antiparallel arrangements of the polymers are seen in the crystal, there are two ways the interpolymer residues could cluster as illustrated in Figure 4B,D. After further examination of these potential sites, we added residues Glu8, Glu9, Glu15, His16, Lys23, Thr27, Ser34, Glu35, Lys56, and Lys63 to our list of potential zinc binding residues.

To test the importance of the selected residues in zinc binding, each residue was changed individually to alanine, and the mutants were assessed for zinc binding. The mutant proteins were incubated in 1 mM EDTA for 36 h, then dialyzed into a solution of 1 mM zinc acetate, and then dialyzed extensively against zinc-free buffer. Finally, the molar zinc occupancy of each mutant protein was determined by ICP-MS.

No single mutation eliminated zinc binding, consistent with the possibility of more than one zinc binding site. Nevertheless, of the 15 single mutants tested, 5 showed somewhat diminished Zn occupancy: H3A, H16A, C20A, H38A, C60A (Figure 5A). C20A, located in a potential site between polymers, showed the largest drop in zinc occupancy. Notably, C20S appeared as a frequent mutation that rendered DGK δ SAM soluble in a previous *in vivo* soluble mutant selection (17). To eliminate Zn binding, we therefore combined the single mutations that reduced occupancy. As shown in Figure 5A, by combining H3A, C20A, H38A, and C60A, we were able to reduce zinc retention to 3%. We define the zinc binding deficient quadruple mutant as DGK δ SAM^{ZnMut}.

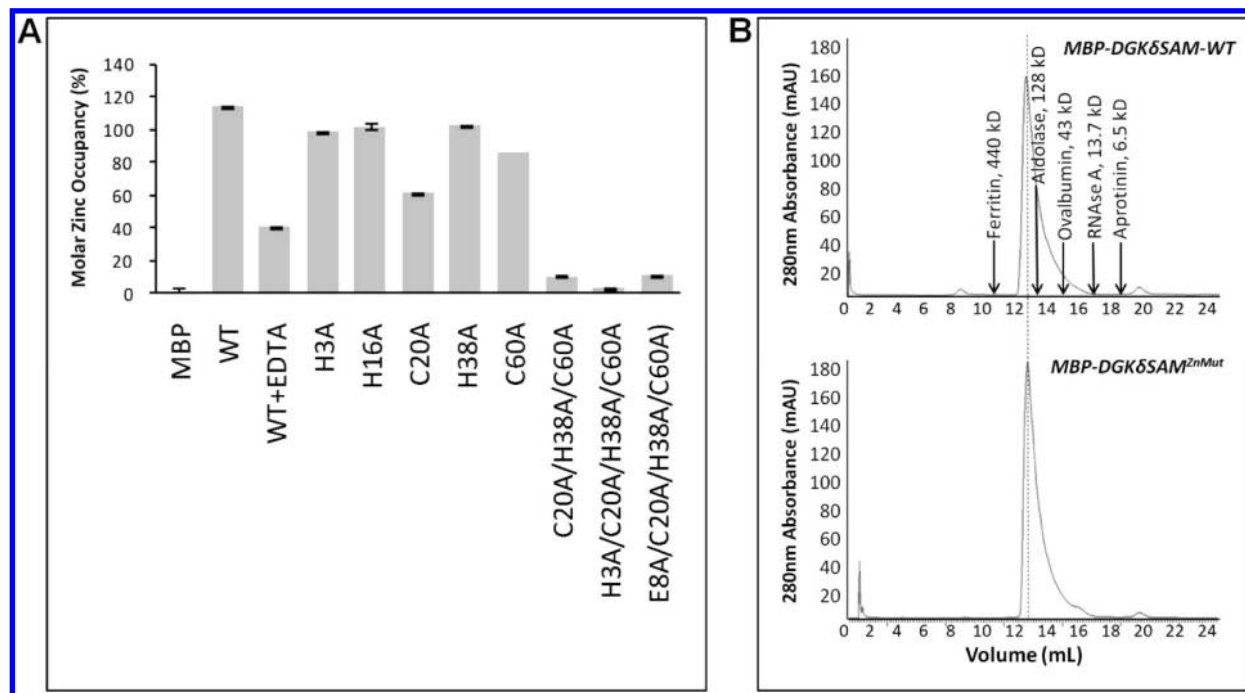


FIGURE 5: Residues involved in DGK δ SAM zinc binding. (A) Zinc binding by DGK δ SAM mutants. MBP-fusion constructs of DGK δ SAM-WT or those containing alanine substitutions were incubated in the presence of 1 mM zinc acetate and dialyzed extensively against zinc-free buffer. Samples were then analyzed by ICP-MS to measure the amount of retained metal. The percent molar zinc occupancy is shown. (B) DGK δ SAM^{ZnMut} has similar self-association properties as the wild-type protein in the absence of zinc. MBP-DGK δ SAM-WT and MBP-DGK δ SAM^{ZnMut} samples were applied to a gel filtration column after incubation with 1 mM EDTA. The two samples are virtually superimposable except for the presence of a small peak in the void volume of the wild-type profile.

As expected, the DGK δ SAM^{ZnMut} construct does not show any increase in turbidity after incubation with 50 μ M zinc acetate, further indicating the importance of zinc in sheet formation (not shown). Moreover, EM images of DGK δ SAM^{ZnMut} showed a minimal effect of zinc on oligomerization (Figure 3E). In the absence of zinc, short polymers are observed for DGK δ SAM^{ZnMut}, much like the wild-type protein. When zinc is added to the DGK δ SAM^{ZnMut}, however, polymers increase in prevalence and length marginally, but no large sheet structures are formed in 50 μ M zinc. Thus, the DGK δ SAM^{ZnMut} appears to be largely refractory to the effects of zinc.

DGK δ SAM^{ZnMut} Can Still Form Polymers in the Absence of Zinc. As shown in Figure 5B, MBP-DGK δ SAM^{ZnMut} protein migrated through a gel filtration column at an elution volume similar to the wild-type protein without zinc, consistent with an average molecular mass of 171 kDa, or roughly 3.3 subunits. Thus, both the WT and DGK δ SAM^{ZnMut} MBP fusion proteins at the same concentration form similarly sized small oligomers in the absence of zinc, consistent with the EM results (above). The MBP fusion constructs form smaller oligomers compared to their tag-free counterparts most likely due to steric inhibition of continued polymer growth imparted by the bulky MBP protein.

Because H38A is near the polymer interface, we also tested the effect of this mutation on subunit affinity by surface plasmon resonance (SPR). We previously reported the K_d of the interaction at the wild-type polymer interface to be $6.3 \pm 1.2 \mu$ M (17). We repeated these experiments in the presence of EDTA and found a slightly increased K_d of $12.2 \pm 2.3 \mu$ M (Figure 6). In comparison, the K_d of an interface that includes the H38A mutation is $23.0 \pm 5.2 \mu$ M. Thus, the affinity of the polymer interface is only minimally altered by the presence of the H38A

mutation. We note that EDTA is insufficient to completely strip zinc from MBP-DGK δ SAM constructs as shown in Figure 5A. Thus, the affinity we obtain for the interface must be evaluated with the caveat that the wild-type protein population will be contaminated with a small fraction of protein bound to zinc.

The DGK δ SAM^{ZnMut} Has Altered Enzyme Localization. To assess the possible physiological role of DGK δ SAM zinc binding, we tested DGK δ SAM^{ZnMut} in the context of the full-length protein in a series of cell biology assays. GFP-DGK δ 1-WT and GFP-DGK δ 1^{ZnMut} fusion constructs were transiently transfected into HEK293 cells. In the absence of TPA stimulation the mutant protein showed a decreased ability to localize to large cytoplasmic puncta (Figure 7A,B). As DGK δ 2 protein has been previously shown to partially colocalize with clathrin (10), we transiently cotransfected GFP-DGK δ 1-WT and mCherry-Clathrin but did not see a significant colocalization of the observed puncta, leaving the identity of DGK δ 1 puncta in HEK293 cells unknown (Supporting Information Figure S3).

To test the effect of the DGK δ SAM^{ZnMut} on signaling, we tested the response to TPA stimulation. TPA is a nonmetabolizable DG analogue that has been previously shown to relocate DGK δ 1 protein to the plasma membrane (8). Populations of GFP-DGK δ 1 transfected cells were stimulated with a TPA gradient from 0.15 to 1.05 μ M. At low and intermediate TPA concentrations, the zinc binding deficient construct displayed a slightly increased propensity to relocate to the plasma membrane relative to the wild-type protein. At 0.45 μ M TPA, most cells expressing the GFP-DGK δ 1-WT construct have lost cytosolic puncta although a large percentage of the protein remains in the cytosol with an average PM-region to cytosolic-region fluorescence intensity ratio of 0.62 ± 0.18 . In comparison, a greater proportion of the GFP-DGK δ 1^{ZnMut} protein appears

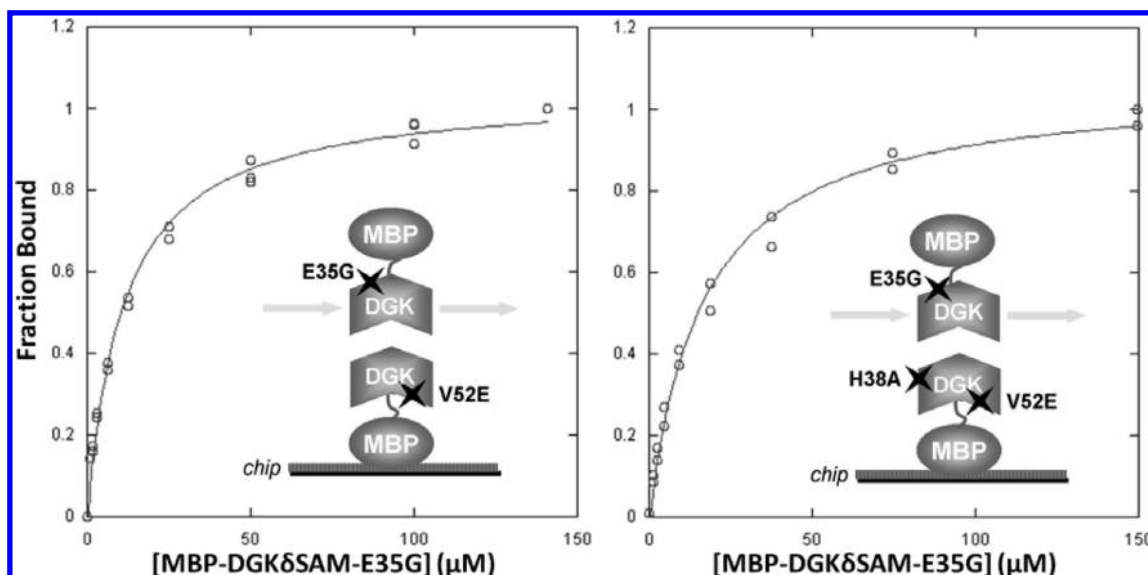


FIGURE 6: H38A, a zinc binding substitution in the intrapolymer interface, does not significantly impact polymer association in the absence of zinc. To measure the affinity between subunits in the polymer, without complications from polymerization, we measured binding between a mutant (V52E) that blocks the EL surface and a mutant (E35G) that blocks the ML surface. This leaves an intact ML surface on the V52E mutant and an intact EH surface on the E35G mutant for binding. Here, either MBP-DGK δ SAM-V52E or MBP-DGK δ SAM-H38A/V52E was immobilized on an SPR chip, and various concentrations of MBP-DGK δ SAM-E35G were applied to the chips. The equilibrium SPR response was measured. The resulting binding curves are shown. The curves were fit to a hyperbolic binding isotherm.

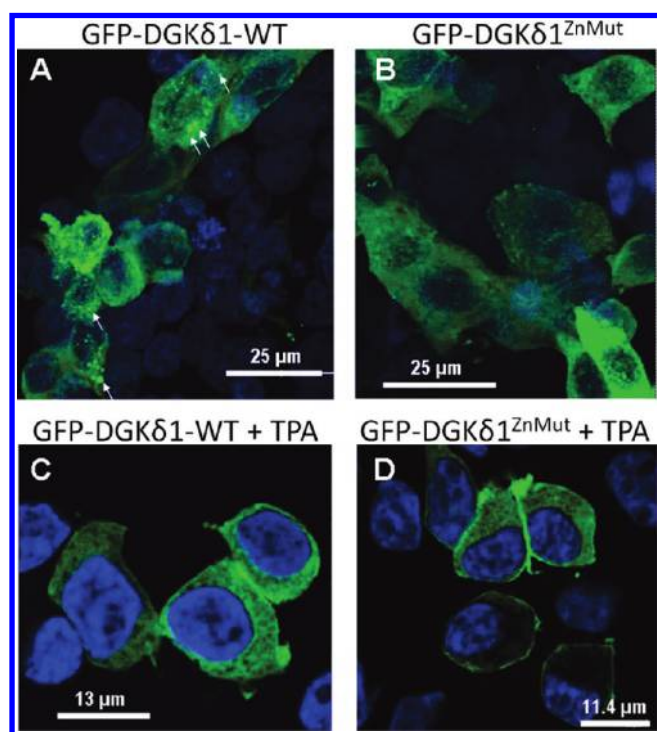


FIGURE 7: Zinc site mutations impair DGK δ 1 localization to cytoplasmic puncta and enhance localization the plasma membrane. (A, B) Projections through HEK293 cells transiently transfected with GFP-DGK δ 1 constructs. The GFP-DGK δ 1-WT construct forms large cytoplasmic puncta (several are indicated by white arrows), which are reduced or absent when the zinc site mutations are introduced. (C, D) Single images of HEK293 cells transiently transfected with GFP-DGK δ 1 constructs followed by incubation with 0.45 μ M TPA. Cells transfected with the DGK construct containing the zinc site mutations show an enhanced propensity to localize to the plasma membrane. Additional images are shown in Supporting Information Figure S4.

to localize to the plasma membrane with a ratio of 1.19 ± 0.19 (Student's two-tailed t test p -value: 1.06×10^{-8}). Figure 7C,D

shows cells representative of the population average. A montage of these cell images is presented in Supporting Information Figure S4.

DGK δ 1-Mediated Inhibition of CopII-Coated Vesicle Formation. DGK δ 1 has been shown to localize to the surface of the ER (11), and it seems reasonable to speculate that a sheet structure could be appropriate for localization or activity at membrane surfaces. Overexpression of DGK δ 1 can inhibit anterograde ER to Golgi transport and has been shown to specifically prevent the formation of CopII-coated vesicles. This function requires both the PH and SAM domains. In order to assess whether zinc binding is involved in ER to Golgi transport regulation, we transiently transfected a number of GFP-DGK δ 1 constructs into a Cos7 cell line stably expressing Sec13-YFP, a marker that localizes to CopII-coated vesicles (Figure 8). As demonstrated previously, overexpression of GFP-DGK δ 1-WT prevents formation of CopII-coated vesicles, visualized as a loss of YFP puncta in cells expressing the GFP-wild-type DGK fusion while Sec13-YFP puncta are still clearly visible in large numbers in surrounding cells without a GFP signal (Figure 8A). Deletion of the SAM domain neutralizes this effect (Figure 8B). The introduction of mutations that block polymerization (V52E) or eliminate zinc binding (DGK δ SAM^{ZnMut}) into the DGK δ 1 construct achieves an effect similar to complete deletion of the SAM domain (Figure 8C,D). These results suggest that regulation of CopII-coated vesicle formation requires a fully functional SAM domain, one with the ability to both polymerize and bind zinc.

DISCUSSION

The DGK δ SAM domain was previously shown to inhibit activity at the plasma membrane by retaining the protein in a cytoplasmic, vesicular localization through its ability to form helical SAM polymers (17). In this study we demonstrate that DGK δ SAM binds zinc with at least two binding sites, one near the polymer interface and one on the surface of the polymer, which appears to drive the side-by-side association of the

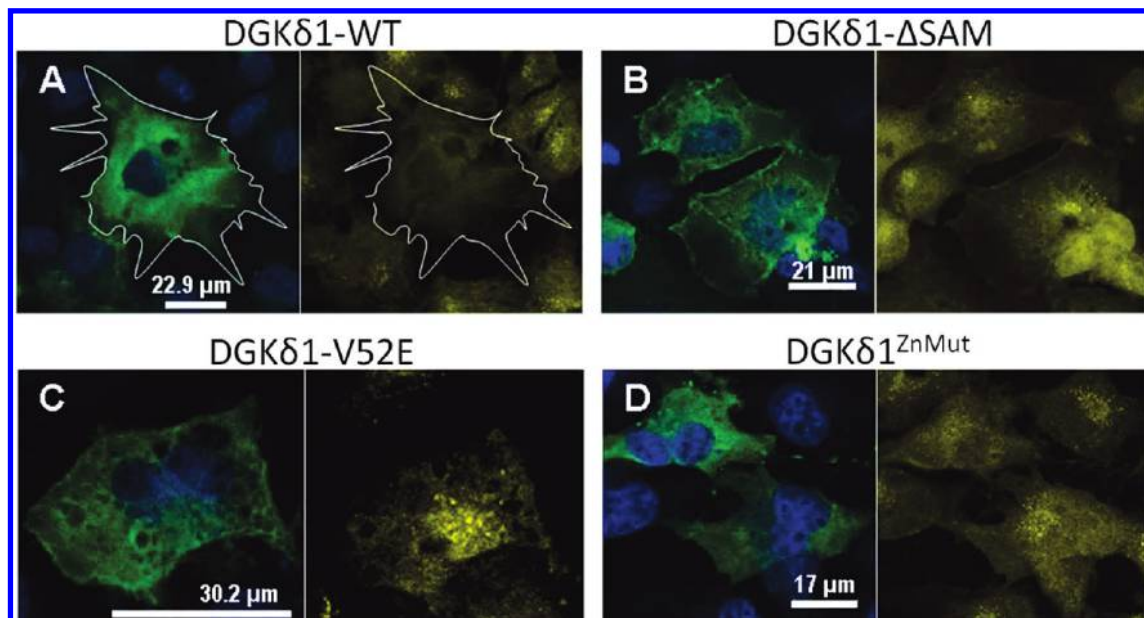


FIGURE 8: Zinc binding mutations impair DGK δ 1 inhibition of CopII-coated vesicle formation. Cos7 cells stably expressing Sec13-YFP, a marker for CopII-coated vesicles, were transiently transfected with GFP-DGK δ 1 constructs. Each set of images shows the overlapping signals for Dapi (blue) and GFP (green) at the left and the YFP signal (yellow) at the right. Cells displaying CopII vesicle formation are peppered with small puncta. White arrows indicate a few representative examples of such puncta. (A) GFP-DGK δ 1-WT expression is mutually exclusive with the formation of Sec13-YFP puncta. A cell strongly expressing the DGK construct is outlined in white and does not contain yellow puncta like its neighboring counterparts which do not express the DGK construct. (B) GFP-DGK δ 1- Δ SAM-expressing cells still show the formation of Sec13-YFP puncta. (C) GFP-DGK δ 1-V52E-expressing cells also show the formation of Sec13-YFP puncta. (D) GFP-DGK δ 1^{ZnMut} expression also does not interfere with the normal formation of Sec13-YFP puncta.

polymers into sheets. Zinc organization and stabilization of DGK δ into two-dimensional sheets may provide an additional level of regulation by helping to maintain an off state of the enzyme, consistent with our finding that disabling zinc binding results in a subtle but significant increase in TPA-stimulated relocalization sensitivity. Zinc has long been known to stabilize the storage form of insulin and may play a similar role in the regulation of DGK δ (26). We cannot entirely exclude, however, the possibility that the mutations that inhibit zinc binding have other effects.

Two-dimensional sheets are an appropriate structure to associate with membrane surfaces. While previous work has shown that the DGK δ 1 population that translocates to the plasma membrane in response to TPA stimulation is mostly monomeric (8), it is possible that the oligomeric form of DGK δ is utilized at other membrane surfaces. Consistent with this idea, we find that mutations that block polymerization or zinc binding eliminate ER localization and DGK δ 1's role in anterograde ER to Golgi transport (11). Low-affinity interactions with lipids or other proteins could be supplemented by the additive effect of polyvalency. Thus, the fact that DGK δ 1^{ZnMut} has lost its ability to form large cytoplasmic puncta may also be the result of the lost avidity for cytoplasmic vesicles.

DGK δ splice variants display overlapping but unique expression profiles across various cell types including high levels in skeletal muscle and testes (4). The zinc content of testes is known to be significantly higher than in other tissues (24). It is possible that this difference in zinc availability might offer the opportunity for DGK δ to fine-tune its behavior in different cell types. In this case, a zinc-induced shift of oligomeric state could serve as a means of further adapting DGK δ behavior to a specific cell type without the need for additional tissue-specific splice variants.

Our results show that both Shank3SAM and DGK δ SAM form zinc-dependent sheets, which suggests that other SAM

domains may possess similar capabilities. The fact that the zinc binding sites are not conserved, however, makes predictions difficult. Nevertheless, zinc binding and sheet formation must be considered as possible roles for other SAM domains.

ACKNOWLEDGMENT

The authors thank Dr. Matthew Schibler and Dr. Martin Phillips for technical support with confocal microscopy and SPR equipment, respectively. The Cos7 cell line stably expressing Sec13-YFP was generously provided by Dr. Ikuo Wada and the mCherry-Clathrin construct by Dr. Klemens Rottner. We also thank Tracy M. Blois, Ryan L. Stafford, and Tyler P. Korman for manuscript review and Hao Li for stock solution preparation.

SUPPORTING INFORMATION AVAILABLE

Supporting Figures S1–S4. This material is available free of charge via the Internet at <http://pubs.acs.org>.

REFERENCES

1. Nishizuka, Y. (2001) Intracellular signaling by hydrolysis of phospholipids and activation of protein kinase C. *Science* 258, 607–614.
2. Luo, B., Regier, D. S., Prescott, S. M., and Topham, M. K. (2004) Diacylglycerol kinases. *Cell. Signal.* 16, 983–989.
3. Sakane, F., Imai, S., Kai, M., Yasuda, S., and Kanoh, H. (2007) Diacylglycerol kinases: why so many of them? *Biochim. Biophys. Acta* 1771, 793–806.
4. Sakane, F., Imai, S., Kai, M., Wada, I., and Kanoh, H. (1996) Molecular cloning of a novel diacylglycerol kinase isozyme with a pleckstrin homology domain and a C-terminal tail similar to those of the EPH family of protein-tyrosine kinases. *J. Biol. Chem.* 271, 8394–8401.
5. Klauk, T. M., Xu, X., Mousseau, B., and Jaken, S. (1996) Cloning and characterization of a glucocorticoid-induced diacylglycerol kinase. *J. Biol. Chem.* 271, 19781–19788.
6. Imai, S., Kai, M., Yasuda, S., Kanoh, H., and Sakane, F. (2005) Identification and characterization of a novel human type II diacylglycerol kinase, DGK κ . *J. Biol. Chem.* 280, 39870–39881.

7. Murakami, T., Sakane, F., Imai, S., Houkin, K., and Kanoh, H. (2003) Identification and characterization of two splice variants of human diacylglycerol kinase ϵ . *J. Biol. Chem.* 278, 34364–34372.
8. Imai, S., Sakane, F., and Kanoh, H. (2002) Phorbol ester-regulated oligomerization of diacylglycerol kinase δ linked to its phosphorylation and translocation. *J. Biol. Chem.* 277, 35323–35332.
9. Sakane, F.; et al. (2002) Alternative splicing of the human diacylglycerol kinase δ gene generates two isoforms differing in their expression patterns and in regulatory functions. *J. Biol. Chem.* 277, 43519–43526.
10. Kawasaki, T., Kobayashi, T., Ueyama, T., Shirai, Y., and Saito, N. (2008) Regulation of clathrin-dependent endocytosis by diacylglycerol kinase δ : importance of kinase activity and binding to AP2 α -phosphatase. *Biochem. J.* 409, 471–479.
11. Nagaya, H., Wada, I., Jia, Y., and Kanoh, H. (2002) Diacylglycerol kinase δ suppresses ER-to-Golgi traffic via its SAM and PH domains. *Mol. Biol. Cell* 13, 302–316.
12. Chibalin, A. V.; et al. (2008) Downregulation of diacylglycerol kinase δ contributes to hyperglycemia-induced insulin resistance. *Cell* 132, 375–386.
13. Kim, C. A.; et al. (2001) Polymerization of the SAM domain of TEL in leukemogenesis and transcriptional repression. *EMBO J.* 20, 4173–4182.
14. Baron, M. K.; et al. (2006) An architectural framework that may lie at the core of the postsynaptic density. *Science* 311, 531–535.
15. Kim, C. A., Sawaya, M. R., Cascio, D., Kim, W., and Bowie, J. U. (2005) Structural organization of a Sex-comb-on-midleg/polyhomeotic copolymer. *J. Biol. Chem.* 280, 27769–27775.
16. Qiao, F., and Bowie, J. U. (2005) The many faces of SAM. *Sci. STKE* 2005, re7.
17. Harada, B. T.; et al. (2008) Regulation of enzyme localization by polymerization: polymer formation by the SAM domain of diacylglycerol kinase δ . *Structure* 16, 380–387.
18. Harding, M. M. (1999) The geometry of metal–ligand interactions relevant to proteins. *Acta Crystallogr., Sect. D: Biol. Crystallogr.* 55, 1432–1443.
19. Harding, M. M. (2000) The geometry of metal–ligand interactions relevant to proteins. II. Angles at the metal atom, additional weak metal–donor interactions. *Acta Crystallogr., Sect. D: Biol. Crystallogr.* 56, 857–867.
20. Harding, M. M. (2001) Geometry of metal–ligand interactions in proteins. *Acta Crystallogr., Sect. D: Biol. Crystallogr.* 57, 401–411.
21. Harding, M. M. (2004) The architecture of metal coordination groups in proteins. *Acta Crystallogr., Sect. D: Biol. Crystallogr.* 60, 849–859.
22. Harding, M. M. (2006) Small revisions to predicted distances around metal sites in proteins. *Acta Crystallogr., Sect. D: Biol. Crystallogr.* 62, 678–682.
23. Berks, B. C. (2008) Biochemistry: cells enforce an ion curtain. *Nature* 455, 1043–1044.
24. Versieck, J., and McCall, J. T. (1985) Trace elements in human body fluids and tissues. *Crit. Rev. Clin. Lab. Sci.* 22, 97–184.
25. Pettit, F. K., Bare, E., Tsai, A., and Bowie, J. U. (2007) HotPatch: a statistical approach to finding biologically relevant features on protein surfaces. *J. Mol. Biol.* 369, 863–879.
26. Dunn, M. F. (2005) Zinc–ligand interactions modulate assembly and stability of the insulin hexamer—a review. *BioMetals* 18, 295–303.